Plateau Regions for Zero-Bias Peaks within 5% of the Quantized Conductance Value $2e^2/h$

Zhaoyu Wang,[1,*] Huading Song,[2,*,†] Dong Pan,[3,*] Zitong Zhang,[1,*] Wentao Miao,[1] Ruidong Li,[1] Zhan Cao,[2] Gu Zhang,[2] Lei Liu,[3] Lianjun Wen,[3] Ran Zhuo,[3] Dong E. Liu,[1,2,4] Ke He,[1,2,4] Runan Shang,[2] Jianhua Zhao,[3,‡] and Hao Zhang[1,2,4,§]

[1]*State Key Laboratory of Low Dimensional Quantum Physics, Department of Physics, Tsinghua University, Beijing 100084, China*
[2]*Beijing Academy of Quantum Information Sciences, 100193 Beijing, China*
[3]*State Key Laboratory of Superlattices and Microstructures, Institute of Semiconductors, Chinese Academy of Sciences, P.O. Box 912, Beijing 100083, China*
[4]*Frontier Science Center for Quantum Information, 100084 Beijing, China*

(Received 18 May 2022; accepted 22 September 2022; published 14 October 2022)

Probing an isolated Majorana zero mode is predicted to reveal a tunneling conductance quantized at $2e^2/h$ at zero temperature. Experimentally, a zero-bias peak (ZBP) is expected and its height should remain robust against relevant parameter tuning, forming a quantized plateau. Here, we report the observation of large ZBPs in a thin InAs-Al hybrid nanowire device. The ZBP height can stick close to $2e^2/h$, mostly within 5% tolerance, by sweeping gate voltages and magnetic field. We further map out the phase diagram and identify two plateau regions in the phase space. Despite the presence of disorder and quantum dots, our result constitutes a step forward toward establishing Majorana zero modes.

DOI: 10.1103/PhysRevLett.129.167702

Majorana zero modes (MZMs) [1,2] have been extensively searched in hybrid semiconductor-superconductor nanowire devices since the first material prediction in 2010 [3,4]. One key prediction, a quantized zero-bias peak (ZBP) in tunneling conductance [5–8], still remains illusive [9–16]. Moreover, theory developments have proposed the concept of quasi-MZMs due to smooth potential variation [17–23] or disorder [24–29]. These quasi-MZMs, though topologically trivial, can also lead to quantized ZBPs. The quantization mechanisms for MZMs and quasi-MZMs are similar: the conductance is solely contributed by one isolated MZM while the second MZM is decoupled. Recent experimental progress has reported large ZBPs whose height can reach $2e^2/h$ [13,14]. However, a single peak at $2e^2/h$ is not enough to be entitled as "quantized." A quantized ZBP requires the peak height sticking to $2e^2/h$ by tuning all relevant experimental knobs: a plateau defined by parameter sweepings. This plateau phenomenon is still missing in experiments.

Here, we have improved the device fabrication and report ZBPs near $2e^2/h$, forming a plateau defined by sweeping gate voltages and magnetic field (B) in an ultrathin InAs-Al nanowire device. We quantify the plateau with a tolerance of 5%, a number commonly used in recent literature [26,27]. In the end, we discuss their possible connections to MZMs or quasi-MZMs.

Figure 1(a) shows the device scanning electron micrograph (SEM). Material and growth details can be found in Refs. [14,30]. The InAs diameter (∼26 nm) is much thinner than those commonly used (∼100 nm), aiming for fewer subband occupations. Theory has shown that fewer or single subband regimes are preferred for MZM quantization [18,31,32]. The device was measured in a dilution fridge, base temperature $T \sim 20$ mK. The electron T can be below 40 mK. A total bias voltage together with a lock-in excitation was applied to contact $N1$ with the current I and dI drained from $S1$. A voltage meter measured V and dV between $N2$ and $S2$. This four-terminal setup can exclude the contributions of contact resistance as a systematic uncertainty. The tunnel gate (TG) and back gate (BG) were used, while side gate (SG) was not well functional and kept grounded. See Fig. S1 in the Supplemental Material for circuit details [33].

The tunneling spectroscopy at zero B [Fig. 1(b)] resolves a hard superconducting gap. The gap size is ∼0.39 mV due to the thin Al film. Figure 1(c) shows the B_z dependence of the gap. The z axis is 8° misaligned with the nanowire. For B along other directions, see Fig. S2. The gap remains hard below 2 T and gradually becomes soft above 3 T. Hard gap at high B is necessary for MZM quantization, since a soft gap destroys the quantization by dissipation [34,35].

In Fig. 1(d), we tune the device to a gate setting and find a ZBP near $2e^2/h$ [see Fig. 1(e) for the waterfall plots]. B is aligned with the nanowire unless specified. Along this direction, the maximum field allowed is 1.87 T due to the hardware limit. From 1.3 to 1.85 T, the zero-bias conductance remains within the 5% tolerance bar, see the pink background (from 0.95 to 1.05). The ZBP width, ∼0.3 mV,

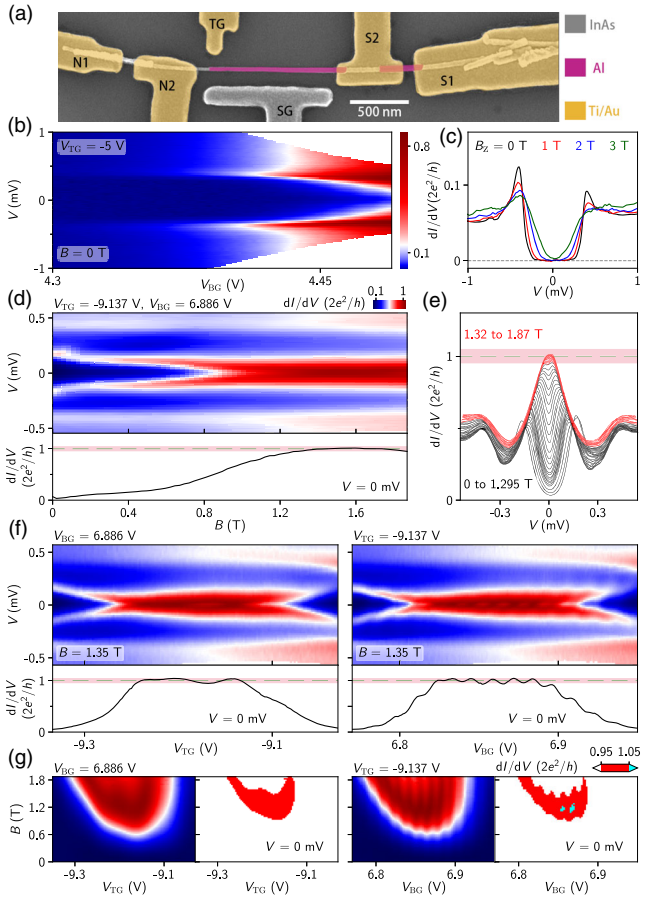

FIG. 1. (a) Device SEM (false colored). The contacts and gates are Ti/Au (5/70 nm in thickness). The substrate is p-doped Si covered by 300 nm thick SiO_2, serving as a global BG. (b) Hard gap tunneling spectroscopy at 0 T. (c) B_z dependence of the gap. (d) B scan (aligned with the nanowire) of a ZBP near $2e^2/h$. Lower panel, zero-bias line cut. The pink bar marks the range from 0.95 to 1.05 in the unit of $2e^2/h$ for all figures. (e) "Waterfall" plots of (d). For clarity, every other line cut is shown and two colors are used. (f) V_{TG} and V_{BG} scans of the ZBP. (g) Gate and B scans at zero bias. The three-color plots mark red as regions within $\pm 5\%$ of $2e^2/h$. (d),(f),(g) Share the same color bar.

is 20 times larger than the thermal width ($3.5k_BT \sim 15$ μeV for $T = 50$ mK). A wide peak is necessary for MZM or quasi-MZM quantization to minimize the effect of thermal broadening. This requires a large tunnel transmission, reflected by the outside gap conductance in Fig. 1(e) being $\sim$10 times larger than that in Fig. 1(c). Large transmission results in a finite subgap conductance. Unlike a soft gap, this Andreev reflection induced subgap conductance does not affect the MZM quantization [35].

We then set B to 1.35 T and scan gate, see Fig. 1(f) (for waterfall plots, see Fig. S3 [33]). The zero-bias conductance remains near $2e^2/h$ over a sizable gate range. Occasionally, it slightly deviates from the 5% tolerance bar due to small oscillations. The oscillations in V_{BG}, also observed in our previous work [14], are possibly due to the formation of an open island, as visualized by the weak Coulomb blockade diamond in the color map. The island is likely defined between the barrier region and the $S2$ contact, which forms a weak barrier due to the ultrathin diameter. The oscillation causes a small splitting of the ZBP, suggesting the energy is also being modified.

The three scans in Figs. 1(d) and 1(f) were in close measurement sequence without noticeable charge jumps in between. These three scans simultaneously pass through one "sweet spot" in the parameter space ($B = 1.35$ T, $V_{TG} = -9.137$ V, $V_{BG} = 6.886$ V), and their zero-bias line cuts all resolve a plateau feature near $2e^2/h$. The plateau in V_{TG} exceeds 100 mV, significantly wider than a fine-tuned sharp crossing. We therefore identify this combined feature as a ZBP plateau near $2e^2/h$, mostly within the 5% tolerance bar.

Figure 1(g) shows the zero-bias map by scanning both B and gate voltages, also passing through this sweet spot. The three-color plots resolve the "red islands" as the $2e^2/h$ regions (within $\pm 5\%$). Occasionally, the conductance can slightly exceed 1.05, by $\sim$1% (the cyan region). The red island is similar to simulations on partially separated MZMs [26]. Based on the Coulomb blockade diamond size $\sim$60 μV and its period in V_{BG} ($\sim$12.7 mV) in Fig. 1(f), we can extract the lever arm between V_{BG} and the energy scale possibly related to the electrochemical potential. The size of the red island in Fig. 1(g) is $\sim$65 mV in V_{BG}, corresponding to an energy scale of $\sim$300 μeV.

In the MZM or quasi-MZM picture, several factors could cause the deviation of ZBP from $2e^2/h$: (1) soft gap, (2) thermal broadening, (3) residual tunnel coupling between the second MZM and the probe, (4) coupling between the two MZMs, and/or (5) multiple subband occupation. The first factor, a soft gap [36], not only destroys ZBP quantization, but is also detrimental to MZM applications [37,38] and should be avoided. This problem has been solved by the observation of a hard gap within the interested B range [Fig. 1(c)]. The second factor lowers the ZBP height. Since our ZBP width is mainly tunnel broadened and $\sim$20 times larger than the thermal width, this effect is also small: thermal averaging at $T = 50$ mK only causes a height change of $\sim$1% for such a wide peak. The third and fourth factors are closely related and can either increase or decrease the height from $2e^2/h$, depending on the coupling details [26]. For the last factor, a second channel could provide a small additional conductance background, increasing the total height above $2e^2/h$ [8]. Based on its saturation conductance (Fig. S2 [33]), our thin nanowire is likely still not in the single subband regime yet. The small zero-bias conductance in Figs. 1(d)–1(g) (at non-ZBP regions), which can be less than 4% of $2e^2/h$, suggests that the multiband contribution to the background conductance (if any) is small.

We next fix V_{TG} to a slightly different value and explore the zero-bias map in (B, V_{BG}) space, see Fig. 2(a).

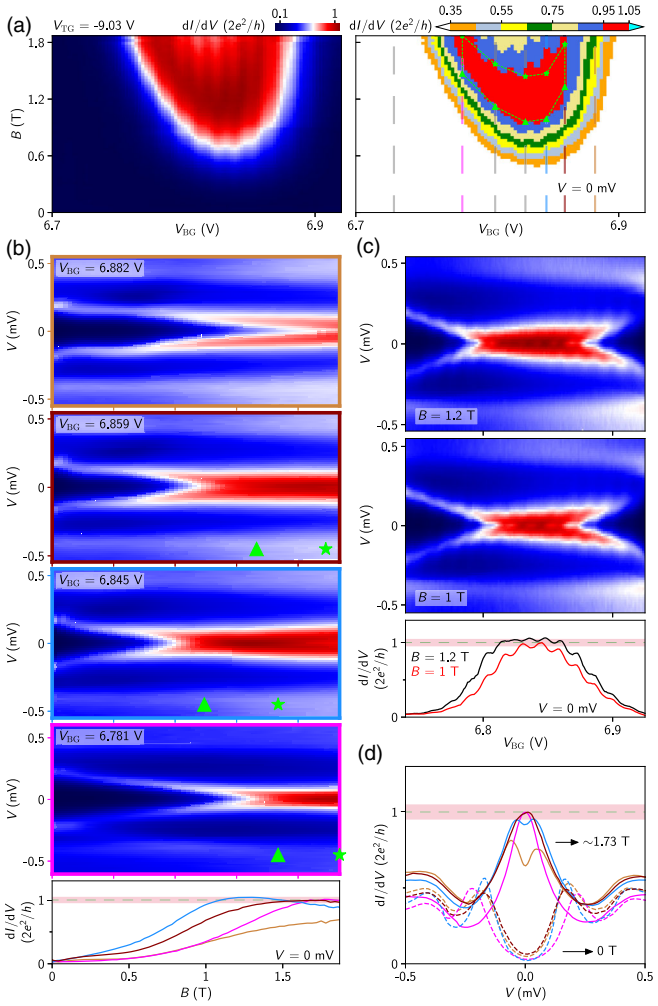

FIG. 2. $V_{TG} = -9.03$ V for all panels. (a) Zero-bias map in (B, V_{BG}) space. Right: the multicolor plot. (b) B scans at four V_{BG} settings, see the dashed lines in (a). Bottom: zero-bias line cuts, with corresponding colors. (c) V_{BG} scan at 1.2 T (top) and 1.0 T (middle) with zero-bias line cuts shown in the bottom. (d) Line cuts from (b) at 0 T (dashed) and ~1.73 T (solid) with corresponding colors. All panels share the same color bar.

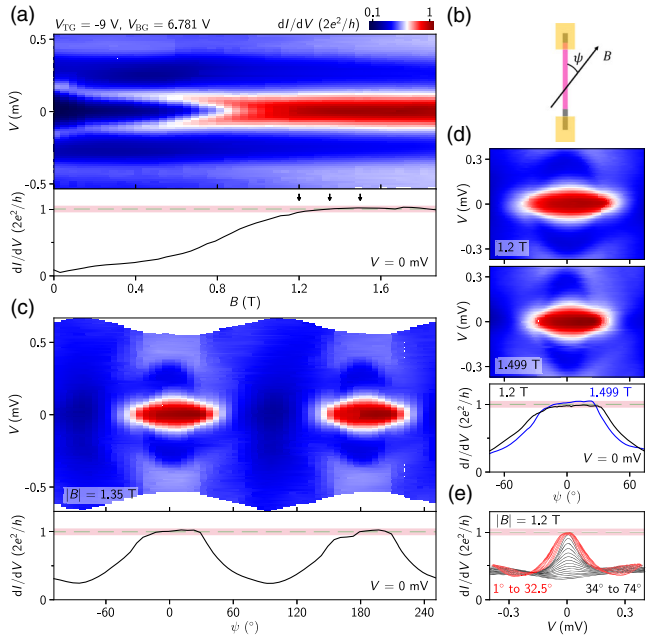

FIG. 3. (a) B scan of a ZBP near $2e^2/h$. Lower: zero-bias line cut. (b) Schematic illustration of the angle ψ. B is in plane. (c) Angle dependence of the ZBP by fixing the B amplitude at 1.35 T, see the middle black arrow in (a). Lower: zero-bias line cut. (d) Two more rotation scans at 1.2 T (upper) and 1.499 T (middle), see the other two arrows in (a). Lower: zero-bias line cuts. (e) Line cuts from (d) (upper). For clarity, half of the angle range (and every other line cut) is shown. All panels share the same color bar.

In addition to the red island as a "zone," we use several discrete colors to label other ranges that are boundarylike. Figure 2(b) shows four B scans; see the corresponding colored dashed lines in Fig. 2(a). The first scan is outside the red island and resolves no ZBPs. Other scans pass through the red island and resolve ZBPs near $2e^2/h$ with different B ranges. The green triangles and stars mark the onset and ending B values for ZBPs. The ZBP region defined by the green dashed lines in Fig. 2(a) roughly matches the red island and can serve as a $2e^2/h$-ZBP phase diagram. Note that not every line cut passing through the red island can resolve a plateau feature. For example, the blue line in Fig. 2(b) is more "peaklike" near $2e^2/h$.

Figure 2(c) shows V_{BG} scans of the ZBP at 1.2 and 1 T, corresponding to the middle and edge of the red island, respectively. The zero-bias line cuts illustrate the evolution from peaklike (red) to plateaulike (black). Figure 2(d) shows the line cuts from the four panels in Fig. 2(b) at $B = 0$ T (dashed lines) and ~1.73 T. At zero field, the subgap peaks have similar energies. At high field (1.73 T), some curves resolve ZBPs near $2e^2/h$, while others resolve split peaks, reflecting the phase diagram boundaries. For waterfall plots and additional scans, see Figs. S3 and S4 [33].

The next experimental knob is the B direction. B rotation in Al-based systems was limited before due to orbital effects: the Al bulk gap is easily suppressed at low B (~0.3 T) during rotation [10]. Here, the ultrathin diameter significantly suppresses the orbital effect and the gap can survive at high B even if misaligned (see Fig. S2 [33]). This advantage enables a rotation for ZBP [39].

Figure 3(a) starts with a B scan (aligned with the nanowire) of a ZBP near $2e^2/h$ (note the minor charge jump at ~1.7 T). The B amplitude is then fixed at three values, see the arrows. Its direction, defined by the angle ψ [Fig. 3(b)], is rotated. B is in plane during rotation (parallel to the substrate). Figure 3(c) shows the angle dependence at 1.35 T. The ZBP remains close to $2e^2/h$ over an angle range of ~50°. Outside this range, the ZBP height quickly decreases away from $2e^2/h$, accompanied by a gap closing. Finally, the ZBP vanishes at larger angles. For $\psi \sim 170°$,

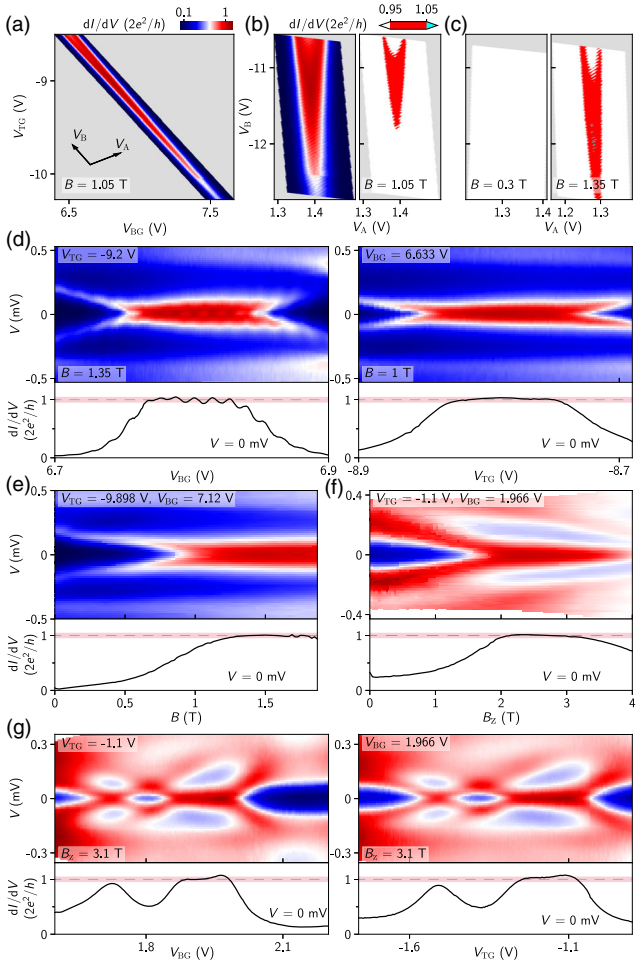

FIG. 4. (a) Zero-bias map in (V_{TG}, V_{BG}) space at 1.05 T. Gray regions have no data. (b) Replotting (a) using the new axis V_A and V_B (see labeling). Right: three-color plot. (c) Zero-bias maps at 0.3 and 1.35 T in three-color plots. (d),(e) Three additional example scans (V_{BG}, V_{TG}, B) for ZBPs within region I. (f),(g) B_z and gate scans of a ZBP in region II. All panels share the same color bar.

the zero-bias conductance drops slightly below $0.95 \times 2e^2/h$ due to a small peak splitting, which is separated by a minor charge jump. Figure 3(d) shows the angle dependence at two other B values, with line cuts shown in Fig. 3(e). For more rotation scans, see Fig. S5 in the Supplemental Material [33].

For the last experimental check, we fix B (aligned with the nanowire) at 1.05 T, and measure the zero-bias map in (V_{TG}, V_{BG}) space, see Fig. 4(a). Because of the crosstalks between the two gates, every gate can tune both the tunnel transmission in the barrier region and the electrochemical potential in the proximitized wire. Therefore, the V_{BG} range is adjusted simultaneously for different V_{TG} settings to trace the same feature. To save space from the "no-data" region (gray), we define new gate voltage axes: $V_A = V_{BG} \cos\phi + V_{TG} \sin\phi$ and $V_B = -V_{BG} \sin\phi + V_{TG} \cos\phi$. $\phi = 30°$. Figure 4(b) replots Fig. 4(a) in (V_A, V_B) axes. Together with Fig. 4(c), the three-color plots show the gradual evolution of the red island: its area increases from none at low B to a sizable zone at high B. For a complete evolution, see Fig. S6 [33]. Figures 4(d) and 4(e) show three additional examples of ZBP scans within this parameter region.

So far, all the ZBPs [from Figs. 1(d)–4(e)] are within one single region (region I) in the multidimensional parameter space (B, V_{TG}, V_{BG}); see Fig. S7 for additional scans in this region [33]. The measurement in region I lasts for three weeks with several charge jumps in between. We note the effects of jumps and hysteresis mainly shift the gate voltages, maximally by 300 mV. The main plateau features still remain after the shift with minor variations.

Figures 4(f) and 4(g) demonstrate another plateau region (region II) at a very different (B, V_{TG}, V_{BG}) setting from region I. To access higher B values, we apply B along the fridge z axis (B_z). The small misalignment (8°) between B_z and the nanowire should not bring a big difference based on the rotation experiment in Fig. 3. In Fig. 4(f), the zero-bias conductance can stick close to $2e^2/h$ from 2 to 3.28 T, a B range larger than 1.2 T (with a tolerance of 5%). Outside this range, the ZBP height drops continuously from $2e^2/h$ with a faster decreasing rate, possibly due to the combined effects of gap closing and softening for B larger than 3 T. The fridge base T for Fig. 4(f) is slightly higher (can reach ~30 mK), which may also play a role. Even within the plateau region, there is still a decreasing trend with a much smaller slope, possibly due to those mechanisms above.

The overall conductance (barrier transmission) in region II is higher than that in region I, leading to a larger subgap conductance. Figure 4(g) illustrates the interaction between the zero-energy state and a quantum dot level, possibly formed near the barrier. Tuning the dot level toward zero energy causes the splitting of the ZBP, similar to the behavior of partially separated MZMs [40,41]. We translate the plateau width in V_{BG} to an energy scale of ~260 μeV based on our extracted lever arm. For additional scans of region II, see Fig. S8 [33]. Though the plateau regions (I and II) in gate voltage space is small, only 50–100 mV, its corresponding energy scale, ~260–300 μeV, is much larger than the thermal energy.

We note that this Letter addresses the question of whether ZBP plateaus near $2e^2/h$ exist by sweeping all relevant experimental parameters. It, however, cannot answer the question of whether similar plateaus (for sweeping all parameters) also exist at nonquantized values. That would require exhausting the entire parameter space in more devices. Based on the collected data so far, we have not observed similar plateaus at other values yet. See Fig. S9 [33] for additional ZBP data due to quantum dots and disorder in regions beyond I and II. Occasionally, we could find plateaulike features above $2e^2/h$ for one-parameter sweeping (but not all). We notice that, for multiple subband occupation, even the MZM could lead

to some plateaulike features above $2e^2/h$ in the open barrier regime with slight disorder [8]. Finally, we compare some scans in Fig. S10 [33] to illustrate the interplay between the barrier transmission and the ZBP height.

To summarize, we have observed ZBPs near $2e^2/h$, which form a plateau mostly within 5% tolerance by sweeping gate voltages and magnetic field. Our result is qualitatively consistent with the (multisubband) MZM as well as quasi-MZM theories: the first is topological while the second is trivial and caused by nonuniform potential or disorder. The quasi-MZM scenario is probably more likely. This work is from a single device whose quality is an improvement compared to our previous one [14], but still not in the ballistic regime yet due to the obvious presence of quantum dots and disorder. In addition to the "end-to-end" correlation experiment to reveal gap closing and reopening [42–44], future devices on "single-terminal" experiments could aim at (1) looking for zero-bias peak-to-dip transition near $2e^2/h$ with better tolerance [14,16,19], (2) using a dissipative probe to reveal quantized ZBPs and suppress others [45–49], and (3) exploring potentially better material systems [50,51].

Raw data for this Letter are openly available from the Zenodo repository [52].

We thank Leo Kouwenhoven for comments. This work is supported by Tsinghua University Initiative Scientific Research Program, Alibaba Innovative Research Program, National Natural Science Foundation of China (Grants No. 12104053, No. 92065106, No. 92065206, No. 61974138, No. 12004040, No. 11974198). D. P. also acknowledges the support from Youth Innovation Promotion Association, Chinese Academy of Sciences (No. 2017156, No. Y2021043).

*These authors contributed equally to this work.
†songhd@baqis.ac.cn
‡jhzhao@semi.ac.cn
§hzquantum@mail.tsinghua.edu.cn

[1] N. Read and D. Green, Paired states of fermions in two dimensions with breaking of parity and time-reversal symmetries and the fractional quantum Hall effect, Phys. Rev. B **61**, 10267 (2000).
[2] A. Y. Kitaev, Unpaired Majorana fermions in quantum wires, Phys. Usp. **44**, 131 (2001).
[3] R. M. Lutchyn, J. D. Sau, and S. Das Sarma, Majorana Fermions and a Topological Phase Transition in Semiconductor-Superconductor Heterostructures, Phys. Rev. Lett. **105**, 077001 (2010).
[4] Y. Oreg, G. Refael, and F. von Oppen, Helical Liquids and Majorana Bound States in Quantum Wires, Phys. Rev. Lett. **105**, 177002 (2010).
[5] K. Sengupta, I. Žutić, H.-J. Kwon, V. M. Yakovenko, and S. Das Sarma, Midgap edge states and pairing symmetry of quasi-one-dimensional organic superconductors, Phys. Rev. B **63**, 144531 (2001).
[6] K. T. Law, P. A. Lee, and T. K. Ng, Majorana Fermion Induced Resonant Andreev Reflection, Phys. Rev. Lett. **103**, 237001 (2009).
[7] K. Flensberg, Tunneling characteristics of a chain of Majorana bound states, Phys. Rev. B **82**, 180516(R) (2010).
[8] M. Wimmer, A. Akhmerov, J. Dahlhaus, and C. Beenakker, Quantum point contact as a probe of a topological superconductor, New J. Phys. **13**, 053016 (2011).
[9] V. Mourik, K. Zuo, S. M. Frolov, S. Plissard, E. P. Bakkers, and L. P. Kouwenhoven, Signatures of Majorana fermions in hybrid superconductor-semiconductor nanowire devices, Science **336**, 1003 (2012).
[10] M. Deng, S. Vaitiekėnas, E. B. Hansen, J. Danon, M. Leijnse, K. Flensberg, J. Nygård, P. Krogstrup, and C. M. Marcus, Majorana bound state in a coupled quantum-dot hybrid-nanowire system, Science **354**, 1557 (2016).
[11] F. Nichele, A. C. C. Drachmann, A. M. Whiticar, E. C. T. O'Farrell, H. J. Suominen, A. Fornieri, T. Wang, G. C. Gardner, C. Thomas, A. T. Hatke, P. Krogstrup, M. J. Manfra, K. Flensberg, and C. M. Marcus, Scaling of Majorana Zero-Bias Conductance Peaks, Phys. Rev. Lett. **119**, 136803 (2017).
[12] Ö. Gül, H. Zhang, J. D. Bommer, M. W. de Moor, D. Car, S. R. Plissard, E. P. Bakkers, A. Geresdi, K. Watanabe, T. Taniguchi *et al.*, Ballistic Majorana nanowire devices, Nat. Nanotechnol. **13**, 192 (2018).
[13] H. Zhang *et al.*, Large zero-bias peaks in InSb-Al hybrid semiconductor-superconductor nanowire devices, arXiv:2101.11456.
[14] H. Song, Z. Zhang, D. Pan, D. Liu, Z. Wang, Z. Cao, L. Liu, L. Wen, D. Liao, R. Zhuo, D. E. Liu, R. Shang, J. Zhao, and H. Zhang, Large zero bias peaks and dips in a four-terminal thin InAs-Al nanowire device, Phys. Rev. Res. **4**, 033235 (2022).
[15] E. Prada, P. San-Jose, M. W. de Moor, A. Geresdi, E. J. Lee, J. Klinovaja, D. Loss, J. Nygård, R. Aguado, and L. P. Kouwenhoven, From Andreev to Majorana bound states in hybrid superconductor–semiconductor nanowires, Nat. Rev. Phys. **2**, 575 (2020).
[16] H. Zhang, D. E. Liu, M. Wimmer, and L. P. Kouwenhoven, Next steps of quantum transport in Majorana nanowire devices, Nat. Commun. **10**, 5128 (2019).
[17] G. Kells, D. Meidan, and P. W. Brouwer, Near-zero-energy end states in topologically trivial spin-orbit coupled superconducting nanowires with a smooth confinement, Phys. Rev. B **86**, 100503(R) (2012).
[18] E. Prada, P. San-Jose, and R. Aguado, Transport spectroscopy of *NS* nanowire junctions with Majorana fermions, Phys. Rev. B **86**, 180503(R) (2012).
[19] A. Vuik, B. Nijholt, A. Akhmerov, and M. Wimmer, Reproducing topological properties with quasi-Majorana states, SciPost Phys. **7**, 061 (2019).
[20] C. Moore, C. Zeng, T. D. Stanescu, and S. Tewari, Quantized zero-bias conductance plateau in semiconductor-superconductor heterostructures without topological Majorana zero modes, Phys. Rev. B **98**, 155314 (2018).
[21] F. Peñaranda, R. Aguado, P. San-Jose, and E. Prada, Quantifying wave-function overlaps in inhomogeneous Majorana nanowires, Phys. Rev. B **98**, 235406 (2018).

[22] Z. Cao, H. Zhang, H.-F. Lü, W.-X. He, H.-Z. Lu, and X. C. Xie, Decays of Majorana or Andreev Oscillations Induced by Steplike Spin-Orbit Coupling, Phys. Rev. Lett. **122**, 147701 (2019).
[23] J. Avila, F. Peñaranda, E. Prada, P. San-Jose, and R. Aguado, Non-Hermitian topology as a unifying framework for the Andreev versus Majorana states controversy, Commun. Phys. **2**, 133 (2019).
[24] H. Pan and S. Das Sarma, Physical mechanisms for zero-bias conductance peaks in Majorana nanowires, Phys. Rev. Res. **2**, 013377 (2020).
[25] S. Das Sarma and H. Pan, Disorder-induced zero-bias peaks in Majorana nanowires, Phys. Rev. B **103**, 195158 (2021).
[26] C. Zeng, G. Sharma, S. Tewari, and T. Stanescu, Partially separated Majorana modes in a disordered medium, Phys. Rev. B **105**, 205122 (2022).
[27] Y.-H. Lai, S. D. Sarma, and J. D. Sau, Quality factor for zero-bias conductance peaks in Majorana nanowire, Phys. Rev. B **106**, 094504 (2022).
[28] H. Pan and S. Das Sarma, On-demand large conductance in trivial zero-bias tunneling peaks in Majorana nanowires, Phys. Rev. B **105**, 115432 (2022).
[29] H. Pan, J. D. Sau, and S. Das Sarma, Random matrix theory for the robustness, quantization, and end-to-end correlation of zero-bias conductance peaks in class D ensemble: Searching for Majorana zero modes in disordered quantum dots and wires, Phys. Rev. B **106**, 115413 (2022).
[30] D. Pan, H. Song, S. Zhang, L. Liu, L. Wen, D. Liao, R. Zhuo, Z. Wang, Z. Zhang, S. Yang, J. Ying, W. Miao, R. Shang, H. Zhang, and J. Zhao, In situ epitaxy of pure phase ultra-thin InAs-Al nanowires for quantum devices, Chin. Phys. Lett. **39**, 058101 (2022).
[31] F. Pientka, G. Kells, A. Romito, P. W. Brouwer, and F. von Oppen, Enhanced Zero-Bias Majorana Peak in the Differential Tunneling Conductance of Disordered Multisubband Quantum-Wire/Superconductor Junctions, Phys. Rev. Lett. **109**, 227006 (2012).
[32] D. Rainis, L. Trifunovic, J. Klinovaja, and D. Loss, Towards a realistic transport modeling in a superconducting nanowire with Majorana fermions, Phys. Rev. B **87**, 024515 (2013).
[33] See Supplemental Material at http://link.aps.org/supplemental/10.1103/PhysRevLett.129.167702 for additional data and analysis.
[34] C.-X. Liu, J. D. Sau, and S. Das Sarma, Role of dissipation in realistic Majorana nanowires, Phys. Rev. B **95**, 054502 (2017).
[35] C.-X. Liu, F. Setiawan, J. D. Sau, and S. Das Sarma, Phenomenology of the soft gap, zero-bias peak, and zero-mode splitting in ideal Majorana nanowires, Phys. Rev. B **96**, 054520 (2017).
[36] S. Takei, B. M. Fregoso, H.-Y. Hui, A. M. Lobos, and S. Das Sarma, Soft Superconducting Gap in Semiconductor Majorana Nanowires, Phys. Rev. Lett. **110**, 186803 (2013).
[37] W. Chang, S. Albrecht, T. Jespersen, F. Kuemmeth, P. Krogstrup, J. Nygård, and C. M. Marcus, Hard gap in epitaxial semiconductor–superconductor nanowires, Nat. Nanotechnol. **10**, 232 (2015).
[38] H. Zhang, Ö. Gül, S. Conesa-Boj, M. P. Nowak, M. Wimmer, K. Zuo, V. Mourik, F. K. De Vries, J. Van Veen, M. W. De Moor *et al.*, Ballistic superconductivity in semiconductor nanowires, Nat. Commun. **8**, 16025 (2017).
[39] J. D. S. Bommer, H. Zhang, Ö. Gül, B. Nijholt, M. Wimmer, F. N. Rybakov, J. Garaud, D. Rodic, E. Babaev, M. Troyer, D. Car, S. R. Plissard, E. P. A. M. Bakkers, K. Watanabe, T. Taniguchi, and L. P. Kouwenhoven, Spin-Orbit Protection of Induced Superconductivity in Majorana Nanowires, Phys. Rev. Lett. **122**, 187702 (2019).
[40] E. Prada, R. Aguado, and P. San-Jose, Measuring Majorana nonlocality and spin structure with a quantum dot, Phys. Rev. B **96**, 085418 (2017).
[41] D. J. Clarke, Experimentally accessible topological quality factor for wires with zero energy modes, Phys. Rev. B **96**, 201109(R) (2017).
[42] T. O. Rosdahl, A. Vuik, M. Kjaergaard, and A. R. Akhmerov, Andreev rectifier: A nonlocal conductance signature of topological phase transitions, Phys. Rev. B **97**, 045421 (2018).
[43] H. Pan, J. D. Sau, and S. Das Sarma, Three-terminal nonlocal conductance in Majorana nanowires: Distinguishing topological and trivial in realistic systems with disorder and inhomogeneous potential, Phys. Rev. B **103**, 014513 (2021).
[44] D. Pikulin, B. van Heck, T. Karzig, E. A. Martinez, B. Nijholt, T. Laeven, G. W. Winkler, J. Watson, S. Heedt, M. Temurhan, V. Svidenko, R. Lutchyn, M. Thomas, G. de Lange, L. Casparis, and D. C. Nayak, Protocol to identify a topological superconducting phase in a three-terminal device, arXiv:2103.12217.
[45] D. E. Liu, Proposed Method for Tunneling Spectroscopy with Ohmic Dissipation Using Resistive Electrodes: A Possible Majorana Filter, Phys. Rev. Lett. **111**, 207003 (2013).
[46] D. Liu, Z. Cao, H. Zhang, and D. E. Liu, Revealing the nonlocal coherent nature of Majorana devices from dissipative teleportation, Phys. Rev. B **101**, 081406(R) (2020).
[47] D. Liu, G. Zhang, Z. Cao, H. Zhang, and D. E. Liu, Universal Conductance Scaling of Andreev Reflections Using a Dissipative Probe, Phys. Rev. Lett. **128**, 076802 (2022).
[48] S. Zhang, Z. Wang, D. Pan, H. Li, S. Lu, Z. Li, G. Zhang, D. Liu, Z. Cao, L. Liu, L. Wen, D. Liao, R. Zhuo, R. Shang, D. E. Liu, J. Zhao, and H. Zhang, Suppressing Andreev Bound State Zero Bias Peaks Using a Strongly Dissipative Lead, Phys. Rev. Lett. **128**, 076803 (2022).
[49] Z. Wang, S. Zhang, D. Pan, G. Zhang, Z. Xia, Z. Li, D. Liu, Z. Cao, L. Liu, L. Wen, D. Liao, R. Zhuo, Y. Li, D. E. Liu, R. Shang, J. Zhao, and H. Zhang, Large Andreev bound state zero bias peaks in a weakly dissipative environment, arXiv:2202.09299.
[50] Z. Cao, D. E. Liu, W.-X. He, X. Liu, K. He, and H. Zhang, Numerical study of PbTe-Pb hybrid nanowires for engineering Majorana zero modes, Phys. Rev. B **105**, 085424 (2022).
[51] Y. Jiang *et al.*, Selective area epitaxy of PbTe-Pb hybrid nanowires on a lattice-matched substrate, Phys. Rev. Mater. **6**, 034205 (2022).
[52] Zenodo, 10.5281/zenodo.6546974 (2022).